Frictional forces during pigging of multiphase pipelines

Hendrix, Maurice; den Heijer, A; Breugem, Wim-Paul; Henkes, Ruud

Important note
To cite this publication, please use the final published version (if applicable).
Please check the document version above.

Frictional forces during pigging of multiphase pipelines

M H W Hendrix [1], A den Heijer [1], W-P Breugem [1], R A W M Henkes [1,2]
[1] Delft University of Technology, The Netherlands
[2] Shell Projects & Technology, The Netherlands

ABSTRACT

In this study the frictional force between a pig and the pipe wall is studied by investigating the properties of the sealing disk of the pig. This is done by subjecting the sealing disk to a wall normal force and a frictional force in a lab facility. The experimental results are compared with values obtained by Finite Element Analysis and by a simplified mechanistic model. The obtained results are important for estimating the steady state pig velocity in a pipeline, and thus for the arrival time of the pig. In addition, the results can be used to improve 1D transient pig modelling in a pipeline, where the frictional force is an input parameter.

1   INTRODUCTION

The use of a pig (Pipeline Inspection Gauge) is often part of the operation or maintenance of pipelines in the oil and gas industry: a cylindrical or sometimes spherical object is launched into the pipeline and runs through the pipeline while being propelled by the production fluids [6]. Such pipelines can transport oil/water, dry gas, or multiphases (such as gas/condensate/water). While a conventional pig seals the pipeline completely and will travel with the mixture velocity, a by-pass pig allows part of the production fluids to by-pass the pig, resulting in a lower pig velocity [1]. Figure 1a shows an example of a by-pass pig. The reduction in pig velocity has proven to be beneficial for both inspection and cleaning purposes [3,8,9,10,13]. As the velocity of the by-pass pig is not dictated by the mixture velocity anymore, detailed understanding of the force balance on the pig is needed in order to predict its velocity. In steady state this implies that the driving pressure force of the production fluids balances with the frictional force of the pig with the pipe wall, see Figure 1b. Applying the steady state force balance results in the following equation for the pig velocity [1]:

$$U_{pig} = U_{mix} - \frac{d^2}{D^2} \sqrt{\left(\frac{F_{fric,tot}}{C \frac{\pi}{8} \rho_{mix} D^2} \right)} \tag{1}$$

Here U_{pig} is the pig velocity, U_{mix} is the mixture velocity, ρ_{mix} is the mixture density, D is the pipe diameter, and d is the diameter of the by-pass opening. $C = \Delta p / (0.5 \rho_{mix} U_{bp}^2)$ is the pressure loss coefficient representing the scaled pressure drop Δp over the pig in dimensionless form. Here U_{bp} is fluid velocity in the by-pass. The total friction force balancing the driving pressure force is denoted by $F_{fric,tot}$.
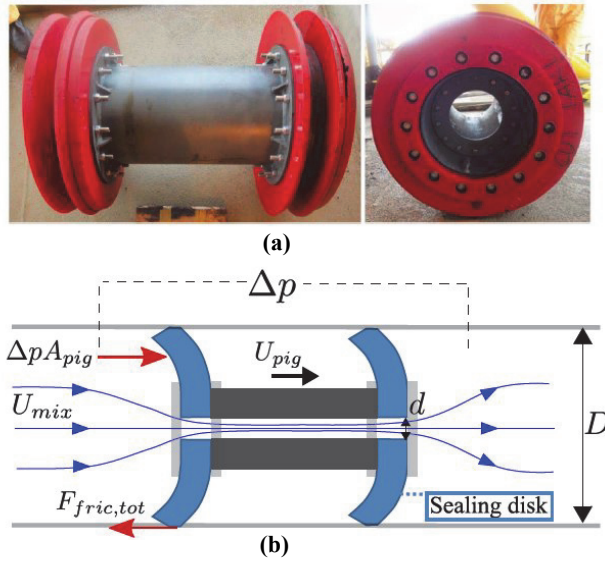
Figure 1: (a) Example of a by-pass pig. Reproduced from [12]. (b) Schematic representation of the force balance on a by-pass pig.

In the past the pressure loss coefficient C of various by-pass pig geometries has been modeled [1,2] to account for the driving pressure force, but so far little attention has been devoted to the quantification and modelling of the frictional force between the pig and the pipe wall [5, 7].

The present study is focused on studying the frictional force during pigging by investigating the properties of the sealing disk of the pig. This is a flexible disk attached to the pig with an oversized diameter relative to the pipe diameter and it is used to fit the pig in the pipeline, see Figure 1b. Since the pig is in contact with the pipe wall via the sealing disk, the properties of this sealing disk have a large influence on the friction force. We define $F_{fric} = F_{fric,tot}/(\pi D)$ as the friction force per meter length of the pipe circumference. An industry rule of thumb is to model F_{fric} as a constant which depends on the type of pig that is being used [4]. For example, a foam pig has a lower F_{fric} than an inspection pig. The constant value of F_{fric} is purely empirical and properties of the sealing disk are not taken into account explicitly in that engineering rule.

The present study is focused on studying the frictional force during pigging in more detail, in which the effect of oversize, thickness of the sealing disk, and material properties of the sealing disk are taken into account. We make use of a simplified model described in [5], which includes properties of the sealing disk, such as the oversize and elastic modulus of the material. We will compare the results of the model with new experimental results obtained in our laboratory. In addition to the simplified model, we perform finite element modelling which is expected to contain more physics, but which also takes more computer time than the simplified model. The results of this study can be used to improve existing correlations [4] for the frictional force on a pig as applied in 1D transient tools (such as OLGA or LedaFlow), which can monitor the propagation of a by-pass pig in a pipeline.

The structure of this paper is as follows. In Section 2 the simplified model for F_{fric} from [5] is explained. This model is compared with experiments carried out in our laboratory, which are discussed in Section 3, and the measurement procedure is given in Section 4. In addition to the experiments, a Finite Element study of the sealing disk is performed, which is explained in Section 5. In Section 6 the results from the simplified model, experiments, and the finite element study will be compared. We conclude and discuss possibilities for future research in Section 7.

2   SIMPLIFIED MODEL

In this section the simplified model from [5] for F_{fric} is explained. The model considers the force balance in a single axisymmetric sealing disk which moves through a pipeline, see Figure 2. The thickness of the disk is denoted by t, the pipe radius is denoted by r, and the radius of the undeformed sealing disk is denoted by r_s. The radius of the spacer disks, which connect the sealing disk to the pig body, is denoted by r_p. Although r_p is not a property of the sealing disk itself, it is an important parameter determining F_{fric} as it defines the part of the sealing disk that is available for bending. As can be noticed from Figure 2a the radius of the sealing disk is larger than the pipe radius. The oversize δ of the sealing disk with respect to the pipe radius is defined as:

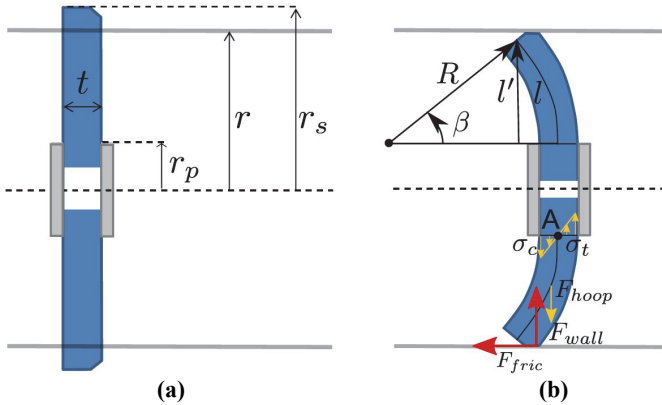$$\delta = \frac{r_s - r}{r} \tag{2}$$

Figure 2: (a) Sketch of an undeformed sealing disk at rest. (b) Sketch of a sealing disk moving inside a pipe.

The simplified model [5] takes a two-step approach. First, the geometry of the moving sealing disk is described. Second, a force balance is applied to this geometry.

It is assumed that the centre line of the sealing disk can be described by an arc with radius R and angle β, see Figure 2b. By assuming that there is no radial compression, the length of the centre line l can be taken constant, i.e. $l = r_s - r_p$. The projected height is denoted as l', which can be related to β:

$$l' = R \sin \beta = \frac{l}{\beta} \sin \beta = \frac{(r_s - r_p)}{\beta} \sin \beta \tag{3}$$

Taking into account the constraint of the pipe geometry, we can also express l' as:

$$l' = r - r_p - \frac{t}{2}\sin\beta \qquad (4)$$

By combining Eq. 3 and Eq. 4 we can solve for β. Since no exact solution exists, β has to be approximated numerically. Note that in this approach we did not take into account the existence of a possible chamfer, which is the worn edge along the sealing disk. For more details, the reader is referred to [5].

With the geometry in place we now consider a moment balance in point A as indicated in Figure 2b. We assume a steady state motion of the pig, which implies that the positive contribution to the moment (red arrows) must be balanced by the negative contribution (yellow arrows). We will now address the different contributions.

The moment in point A caused by F_{fric} is expressed as:

$$M_f = F_{fric}(r - r_p)rd\theta \qquad (5)$$

Here θ is the circumferential coordinate. Recall that the unit of F_{fric} is [N/m], which is the friction force per meter length of the circumference. The wall friction F_{fric} and the wall normal force F_{wall} are related through a coefficient of friction μ as:

$$\mu = \frac{F_{fric}}{F_{wall}} \qquad (6)$$

We can then write the moment in point A caused by F_{wall} as:

$$M_w = F_{wall}\left(R(1 - \cos\beta) - \frac{t}{2}\cos\beta\right)rd\theta = \frac{F_{fric}}{\mu}\left(R(1 - \cos\beta) - \frac{t}{2}\cos\beta\right)rd\theta \qquad (7)$$

To describe the stress-strain relationship we introduce the E-modulus and the Poisson ratio ν, which are material properties of the sealing disk. In this analysis we assume E to be constant. The moment in point A induced by the compression and tension bending stress $\sigma_{c,t}$ can then be expressed as [5]:

$$M_c = M_t = \frac{t^3 E r_p}{24R}d\theta \qquad (8)$$

In addition to the compression and tension bending stress, a hoop stress will have a negative contribution to the moment at point A. The hoop stress is caused by the circumferential compression of the sealing disk. It can be expressed as [5]:

$$M_\theta = E\frac{R^2 t\,d\theta}{1 - \nu^2}\int_0^\beta \frac{\alpha - \sin\alpha}{\alpha + \frac{r_p}{R}}(1 - \cos\alpha)d\alpha \qquad (9)$$

Here α is the angle defined on the interval $[0, \beta]$. The integral can be evaluated numerically. We can now write for the total moment balance around point A:

$$(M_f + M_w) - (M_c + M_t + M_\theta) = 0 \qquad (10)$$

We can solve this equation explicitly for F_{fric}:

$$F_{fric} = \frac{(M_c + M_t + M_\theta)}{(r - r_p)rd\theta + \frac{1}{\mu}\left(R(1 - \cos\beta) - \frac{t}{2}\cos\beta\right)rd\theta} \tag{11}$$

We will test this simplified model against experiments, as explained in the next section.

3   EXPERIMENTAL SETUP

In the previous section it was shown that the deformation of the sealing disk is caused by F_{wall} and F_{fric}, which are balanced by the forces associated with the elastic deformation of the sealing disk. F_{wall} and F_{fric} are related through the coefficient of friction μ, see Eq. 6. The coefficient of friction is a difficult parameter to predict and is not only dependent on the properties of the sealing disk, but also on the properties of the pipe, such as the wall roughness. Also the fluids that are transported in the pipe during the pigging operation can influence the effective coefficient of friction, as the fluids may act as a lubricant. In this study we do not attempt to predict μ, but rather take it as an input parameter to account for the variety in friction coefficients that can be encountered in the field.

To this purpose the following experiment has been designed, see Figure 3. In the experimental setup a sealing disk is subjected to a circumferential force F_1 by reducing the diameter of a hull that is wrapped around the sealing disk, as shown in Figure 2. By applying an energy balance, this force can be linked to the normal force F_{wall} that is exerted by the hull onto the sealing disk as:

$$F_{wall}2\pi r\Delta r = F_1 2\pi\Delta r \tag{12}$$

which results into:

$$F_{wall} = \frac{F_1}{r} \tag{13}$$

By varying the diameter of the hull, which resembles the confining geometry of a pipe, the effective oversize of the sealing disk can be systematically adjusted. In addition, a second force F_2 can be applied perpendicular to the disk. This force can be linked to the friction force per meter length of the circumference, F_{fric}, as:

$$F_{fric} = \frac{F_2}{2\pi r} \tag{14}$$

By changing the ratio F_2/F_1 the friction coefficient can be varied in the experiment:

$$\mu = \frac{F_{fric}}{F_{wall}} = \frac{F_2}{2\pi F_1} \tag{15}$$

F_2, and thus μ, can be varied from 0 up to a maximum value at which the disk starts to slide. In principal, even higher values of μ could have been obtained by fixating the disk to the hull to prevent sliding. This was, however, not done in the current experiment.
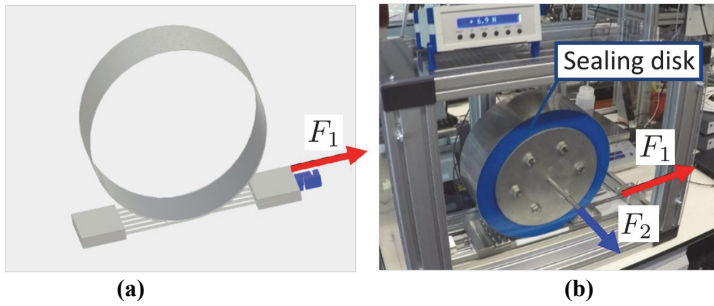
Figure 3: (a) Schematic of the setup. (b) Photograph of the experimental setup with a sealing disk.

4   MEASUREMENT PROCEDURE

All measurements were performed with two 24-bit GSV-2TSD-DI data acquisition devices connected to a 1kN and 2 kN load cell (KD40S, ME-Systeme), for the circumferential (F_1) and for the axial direction (F_2), respectively. The measurements were performed at 10 Hz and logged onto a computer. The measurement procedure starts by placing the sealing disk in the enclosing hull, see Figure 3. Subsequently, the diameter of the hull is reduced to the specified oversize at the start of each measurement, which is kept constant during the remaining course of the measurement. At this point no axial force is applied, so $\mu = 0$. Subsequently, the force in the axial direction (F_2) is increased. When F_2 increases the circumferential force F_1 decreases. The increase in F_2 and decrease in F_1 are shown in Figure 4, where a typical result of a time series is shown as an example. The disk for this case is a 12" disk from vendor X subjected to an oversize of 2.8%. The properties of this disk (disk A) can be found in Table 1 in Section 6. The radius of the spacer disks r_p is kept constant for all experiments at a value of $r_p = 0.086$ m. During the entire measurement the disk is pulled through the hull in steps. At each step three zones are distinguished: a rapid increase in force (rise), a steady constant force (slip) and finally a slow decrease in force (rest), see Figure 4b. These different zones are explained below.

In the rise zone the disk is still in static equilibrium. F_2 is gradually increased, as is showed by the black line in Figure 4b. When the disk starts moving the slip zone is entered, which is shown by the magenta line in Figure 4b. At this point F_2 does not increase anymore, but oscillates, which indicates the transition from static equilibrium to slip motion. Finally, the system is not adjusted anymore and the disk comes at rest which is shown by the green line in Figure 4b. During rest it is seen that both the forces F_1 and F_2 are restored.

The ratio between F_2 and F_1 determines μ, see Eq. 15. As this ratio varies during the experiment, we can calculate the corresponding μ at all time instances, which is shown in Figure 4a. Since we can obtain all values of μ between 0 and some maximum value at which the disk starts to move, this method gives a way to test the behaviour of the sealing disk for different values of μ. This is shown in Figure 4c, where F_1 and F_2 are given as function of μ.
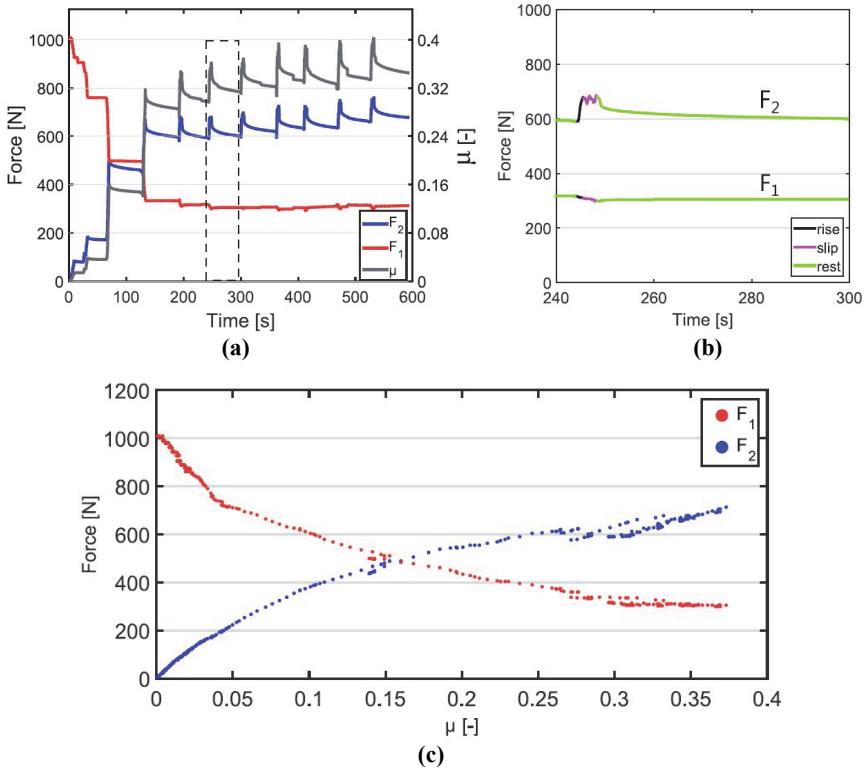
Figure 4: (a) Time series of F_1 and F_2 and the corresponding value for μ. (b) A close up of F_1 and F_2 between 240 and 300 seconds, which is indicated in panel a with the dashed box. (c) F_1 and F_2 plotted for different values μ, including only the points that have been recorded during the rise zone.

Since we are interested in a situation where the disk is in equilibrium, we only select points from the rise part of the time series of F_1 and F_2. We note that as μ is increased, the value of F_2 rises and consequently the value of F_1 drops. This can be expected as the disk is not only supported by a wall normal force (related to F_1) but also by a wall friction force (related to F_2) for a certain μ, see Section 2. By increasing F_2, we will thus expect a decrease of F_1.

We can now extract values of F_1 and F_2 for different values of μ. In the following sections we choose to cast the results in a form which shows F_2, as it is equal to the total friction force that the sealing disk is experiencing. This form is therefore directly relevant for applications and it can be readily compared to other results available in the literature. With F_2 in place, F_1 can in principle directly be obtained using Eq. 15. As a final remark we stress that although the results in this experiment are obtained in a *static* equilibrium, the results are equally valid for a sealing disk *moving* through a pipeline with a given coefficient of sliding friction μ. This is because the same forces apply to a sealing disk of a pig which moves with a constant velocity.

5 FINITE ELEMENT MODEL

The simplified model described in Section 2 assumes a constant value for the E-modulus. This implies that the analytical model holds for linear elasticity with a constant E. By using finite element software (Femap 11.0.0 64-bit) the assumption of linear elasticity is checked by comparing a linear material model against a non-linear Rivlin material model. The Rivlin material model is fitted with the help of a least squares algorithm in Adina 601 to axial strain experiments of an actual sample of the sealing disk. The axial strain experiments have been performed in our laboratory according to ASTM D412.
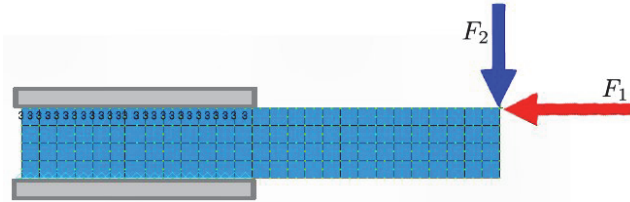

Figure 5: Finite element mesh of a sealing disk in axisymmetric perspective. The two forces F_1 and F_2 are applied as shown. By fixating the ratio between F_2 and F_1 the coefficient of friction μ is imposed.

The finite element model is shown in Figure 5. The dimensions are based on the properties of disk A, which can be found in Table 1. The fixation is modelled by fixating the nodes at the location of the spacer disk in the axial direction. F_1 and F_2 are applied for a range of magnitudes while keeping μ constant. The sealing disk will deform accordingly and will reach an equilibrium at a new maximum radius r, which corresponds to an oversize δ, defined by Eq. 2. In this way the forces corresponding to a specific oversize δ can be obtained from the finite element model.

The geometry is built in Femap 11.0.0 64-bit and solved with the advanced non-linear solver Adina 601. Axisymmetric 2nd order quadrature elements are used. The model has been checked for grid convergence by refining the mesh by a factor 4 from 108 to 432 elements. The forces for F_2 changed by less than 1% when the iteration process was stopped.

Figure 6 shows the result obtained for disk A. In addition to the actual disk thickness of 15 mm, also simulation results for thickness values of 13 and 17 mm are included. The disk in this example has a value of 75 shore hardness, see Table 1. Based on this value for the shore hardness an initial estimate of the E-modulus can be obtained from the Gent equation [11]. As can be seen in Figure 6, the Gent equation underestimates the results predicted by the non-linear material model. Instead of relying on the Gent equation a new E-modulus was fitted by choosing a value which is in agreement with the non-linear material model. For an assumed Poisson ratio of $\nu = 0.45$ an E-modulus of 12.25 MPa is found. A comparison of the finite element results with results obtained from the simplified model and with the experimental results will be given in the next section.
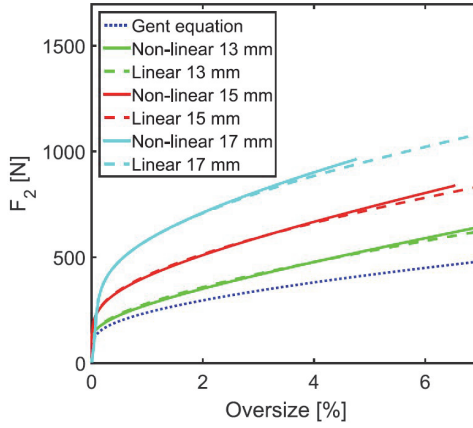
Figure 6: Difference between the linear (solid line) and non-linear (dashed line) material model for a range of thicknesses. Results for the linear model correspond to $E = 12.25$ MPa. The used mesh is shown in Figure 5.

6   RESULTS

In Figure 7 various experimental results are compared with results obtained from the simplified analytical model given by Eq. 11. The disks that have been investigated are listed in Table 1. The letter assigned to each disk in Table 1 corresponds to the letter of the panel in Figure 7. For disk A also finite element results with the non-linear material model are available, as explained in the previous section. This non-linear model is not available for disk B-D, as there were no material tests performed on samples of these sealing disks.

Figure 7a shows a comparison for disk A. To compare the experimental results with the analytical model, F_2 for a constant μ needs to be obtained from the experiment. To obtain data points for $\mu = 0.3$, the average of all values between $\mu = 0.29$ and 0.31 is taken. For example, for an oversize of 2.8% Figure 4 shows that $F_2 \approx 600N$ for disk A. For the analytical model two curves are shown. The red dashed line shows the result for the equivalent E-modulus of 12.25 MPa suggested in Section 5. The red solid line shows the analytical result for an E-modulus that is fitted to the finite element results having a value of $E_{fit} = 17.8$ MPa. We thus conclude that for this disk the analytical model with $E = 12.25$ MPa underpredicts the friction force F_2 by a factor of about 1.45. The trend that higher values of the oversize result in higher values of F_2 is however correctly captured by the model.

Table 1: Properties of the four different sealing disks that were used in the experiments.

Disk	A	B	C	D
Vendor	X	Y	Y	Y
r_s [m]	0.162	0.154	0.154	0.154
t [mm]	15	15	13	15
Material hardness (Shore A)	75	75	75	65
E_{fit} [MPa]	17.8	12.5	12.5	7
μ [-]	0.3	0.25	0.25	0.25

Next we consider disk B with properties summarized in Table 1. Figure 7b shows the result. Since no material tests have been performed disk B, the E-modulus was fitted, and a value of $E_{fit} = 12.5$ MPa was obtained. We remark that the values of F_2 for disk B are smaller than those for disk A shown in Figure 7a, which is also reflected in the lower value of E_{fit}. The shore hardness value of both disks, however, is specified to be 75. This indicates that the shore hardness value of a sealing disk does not provide enough information on the actual value of the E-modulus, and that more information is needed to predict the behaviour of the sealing disk.

With the specified E modulus $E_{fit} = 12.5$ MPa of the 75 shore disk B, we now continue with the results of the same disk, but with a thickness of 13 mm instead of 15 mm (disk C). We intuitively expect that F_2 will be lower, as it is easier to deform a thinner disk than a thicker disk. Indeed this is confirmed by the results shown in Figure 7c. The overall value of F_2 is lower, and the model accurately predicts this with the same $E_{fit} = 12.5$ MPa as has been determined for the 15 mm disk.

Finally, we investigate the behaviour of the same disk B in Table 1, but now with a shore hardness of 65 instead of 75 (disk D). As the material properties have changed, we now have to use a new value for the E-modulus, which is found to be $E_{fit} = 7.0$ MPa. As the disk is softer, we indeed observe lower values for F_2. With the value of E_{fit} in place we observe that the model follows the experimental results reasonably well.
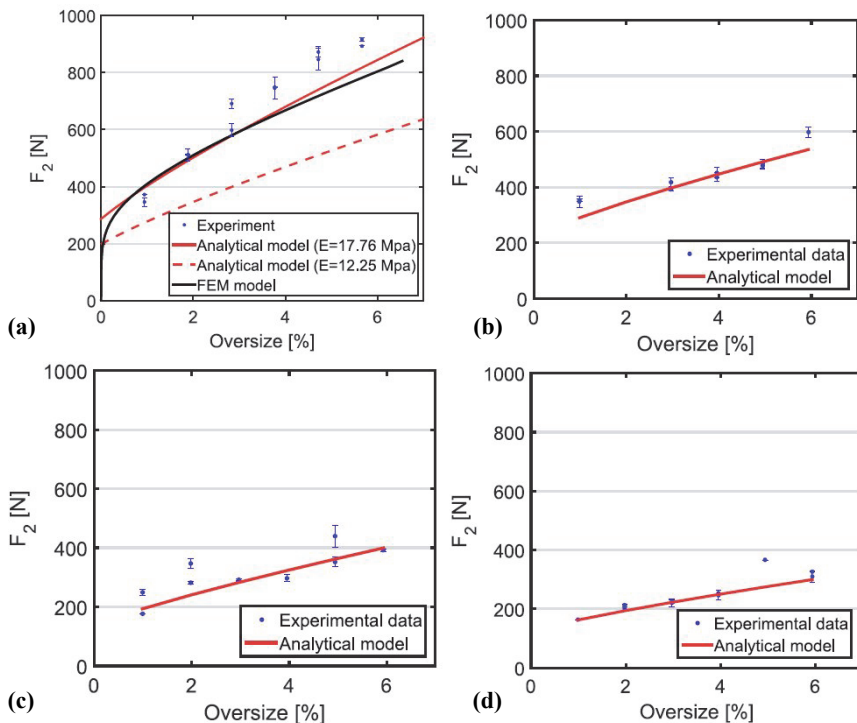

Figure 7: (a-d) Comparison of the analytical model with experimental results. Properties of disk are summarized in Table 1. The letter assigned to each disk in Table 1 corresponds to the letter of the panels in this figure.

7 CONCLUSION

In this paper an experiment has been presented which is able to measure the friction force and wall normal force which act on a sealing disk of a pig in a confined pipe geometry. The coefficient of friction is an input parameter which can be systematically varied. This allows the results to be applied to a pig with such a sealing disk that is moving at constant velocity with the same coefficient of the sliding friction. The oversize has been systematically varied. The experimental results have been compared with predictions from a finite element model which uses a non-linear Rivlin material model that was calibrated using a sample consisting of the same material as the actual sealing disk according to ASTM D412. The results from the finite element model agree reasonably well with the experiments with a maximum error of 18%. In addition, a simplified mechanistic model from the literature was tested against experiments. This simplified model relies on a constant value for the E-modulus. With a fitted equivalent E-modulus, the analytical model was found to perform reasonably well. Sealing disks from different vendors have been compared. It was shown that the value for the Shore hardness alone is not enough to predict the E-modulus that can be used to predict the frictional force of the sealing disk. We therefore recommend carrying out more material tests on sealing disks which will allow for further investigation of the effect of the material properties on the friction force. In that way the range of validity of the analytical model can be further assessed.

REFERENCES

1. Singh A. and Henkes R.A.W.M., "CFD modeling of the flow around a by-pass pig", 8th North American Conference on Multiphase Technology, 2012.
2. Azpiroz J.E., Hendrix M.H.W., Breugem W.-P. and Henkes R.A.W.M., "CFD modelling of bypass pigs with a deflector disk", 17th Int. Conf. on Multiphase Technology, 2015.
3. Entaban A., Ismail A., Jambari M., Ting P., Amin K.M., Ping C.C., Zou S. and Spronsen G. Van, "By-pass pigging - a 'simple' technology with significant business impact", International Petroleum Technology Conference, 2013.
4. Cordell J.L., "Conventional pigs - what to use and why", Pipes and Pipelines International, 1992.
5. O'Donoghue A.F., "On the steady state motion of conventional pipeline pigs using incompressible drive media", PhD. Thesis, 1996.
6. Quarini J. and Shire S., "A review of fluid-driven pipeline pigs and their applications", Journal of Process Mechanical Engineering, 222:1-10, 2007.
7. Zhu X., Wang D., Yeung H., Zhang S. and Liu S., "Comparison of linear and nonlinear simulations of bidirectional pig contact forces in gas pipelines", Journal of Natural Gas Science and Engineering, 27:151-157, 2015.
8. Money N., Cockfield D., Mayo S. and Smith G., "Dynamic speed control in high velocity pipelines", Pipeline & Gas Journal, 239:30-38, 2012.

9. O'Donoghue A., "Pigging as a flow assurance solution − avoiding slug catcher overflow", PPSA Seminar, 2012.

10. Entaban A., Ismail A., Jambari M., Ting P., Amin K.M., Ping C.C., Zou S. and van Spronsen G., "By-pass pigging − a 'simple' technology with significant business impact", International Petroleum Technology Conference, 2013.

11. Gent A., "On the relation between indentation hardness and Young's modulus", Rubber Chemistry and Technology, 31: 896, 1958.

12. Lee H.S., Agustiawan D., Jati K., Aulia M.A.H., Thomas S.A., and Appleyard S.P., "By-pass pigging operation experience and flow assurance study", Offshore Technology Conference, Houston, 2012.

13. Wu H.L., van Spronsen G., "Slug reduction with high by-pass pigs − a mature technology", 12th International Conference on Multiphase Production Technology, Barcelona, 2005.